A&A 473, 715–725 (2007)
DOI: 10.1051/0004-6361:20077926
© ESO 2007

Astronomy & Astrophysics

Effects of the halo concentration distribution on strong-lensing optical depth and X-ray emission

C. Fedeli[1], M. Bartelmann[1], M. Meneghetti[2], and L. Moscardini[3,4]

[1] Zentrum für Astronomie, ITA, Universität Heidelberg, Albert-Überle-Str. 2, 69120 Heidelberg, Germany
e-mail: cosimo@ita.uni-heidelberg.de
[2] INAF – Osservatorio Astronomico di Bologna, via Ranzani 1, 40127 Bologna, Italy
[3] Dipartimento di Astronomia, Università di Bologna, via Ranzani 1, 40127 Bologna, Italy
[4] INFN, Sezione di Bologna, viale Berti Pichat 6/2, 40127 Bologna, Italy

Received 22 May 2007 / Accepted 27 July 2007

ABSTRACT

We use simulated merger trees of galaxy-cluster halos to study the effect of the halo concentration distribution on strong lensing and X-ray emission. Its log-normal shape typically found in simulations favors outliers with high concentration. Since, at fixed mass, more concentrated halos tend to be more efficient lenses, the scatter in the concentration increases the strong-lensing optical depth by $\lesssim$50%. Within cluster samples, mass and concentration have counteracting effects on strong lensing and X-ray emission because the concentration decreases for increasing mass. Selecting clusters by concentration thus has no effect on the lensing cross section. The most efficiently lensing and hottest clusters are typically the *least* concentrated in samples with a broad mass range. Among cluster samples with a narrow mass range, however, the most strongly lensing and X-ray brightest clusters are typically 10% to 25% more concentrated.

Key words. gravitational lensing – galaxies: clusters: general – cosmology: dark matter

1. Introduction

It is widely accepted now that dark-matter halos in both simulations and reality are less concentrated, i.e. have larger relative core sizes, the more massive they are. This is interpreted as a consequence of hierarchical, bottom-up structure formation. More massive halos form later, in a less dense environment, and thus reach lower central densities. The variety of their individual formation histories gives rise to a concentration distribution that simulations show to be approximately log-normal with a standard deviation of $\approx$0.2.

What effects does this fairly broad concentration distribution have on observable properties of galaxy clusters, most notably their strong gravitational lensing cross sections and their X-ray temperatures and luminosities? The log-normal distribution is substantially skewed and allows larger positive than negative deviations from the mean. At fixed halo mass, this should lead to outliers with higher temperature, higher X-ray luminosity, and larger strong-lensing cross sections than expected for the nominal concentration value.

How are such expectations to be extrapolated to cluster samples? Above a given mass limit, halos with lower mass and generally higher concentration are much more abundant than more massive and typically less concentrated halos. Mass and concentration have counter-acting effects on most observables. For example, at fixed concentration, more massive halos are more efficient lenses as well as hotter and more luminous X-ray emitters. However, since the concentration is decreasing with increasing mass, these effects are at least partially reduced.

Here, we study the effect of the concentration distribution on several cluster properties. We use simulated merger trees of cluster-sized, dark-matter halos, for which concentrations are randomly drawn from a log-normal distribution. We focus on three observable quantities, namely the strong-lensing efficiency and the X-ray temperature and luminosity of these clusters, and model all of them with semi-analytic algorithms taking the importance of major mergers into account. As a matter of fact, cluster mergers boost both lensing efficiency and X-ray emission (Torri et al. 2004; Randall et al. 2002).

Earlier studies on the sensitivity of strong lensing to the concentration of dark matter halos and its scatter exist. In particular, Wyithe et al. (2001), Keeton & Madau (2001) and Kuhlen et al. (2004) focused on the statistics of multiple images as a probe of the inner structure of halos, in order to put constraints on the dark matter self-interaction cross section, on the inner slope of the density profile and on the equation of state parameter for dark energy, respectively. In these studies isolated and spherical cluster models were always considered. In Oguri et al. (2001) the effects of the concentration and inner slope of dark matter halos on arc statistics were considered, again assuming axial symmetry for both sources and lenses. Finally, in Hennawi et al. (2007), N-body simulations were used to analyse the dependence of strong lensing cross section on several cluster properties.

The paper is organised as follows. In Sect. 2 we review the properties of the NFW density profile, the relation between mass and concentration and different implementations thereof. In Sect. 3, we specify the construction of the cluster sample used in our calculations and its properties. Section 4 describes our results on the relations between halo concentration, strong-lensing cross sections and optical depths, X-ray temperature and

Article published by EDP Sciences and available at http://www.aanda.org or http://dx.doi.org/10.1051/0004-6361:20077926

luminosity. Finally, we summarise our work in Sect. 5 and discuss the conclusions.

2. Dark matter halos

2.1. Density profile

Quiescent dark-matter halos in N-body simulations acquire density profiles well approximated by the NFW (Navarro et al. 1995) fitting formula (see also Dubinski & Carlberg 1991; Navarro et al. 1996, 1997; Moore et al. 1998; Power et al. 2003; Navarro et al. 2004),

$$\rho(r) = \frac{\rho_\mathrm{s}}{(r/r_\mathrm{s})(1 + r/r_\mathrm{s})^2}. \quad (1)$$

Its two free parameters are the scale radius r_s, where the logarithmic profile slope reaches -2, changing from -3 outside towards -1 inside, and the scale density $\rho_\mathrm{s} = 4\rho(r_\mathrm{s})$. For a dark-matter halo at redshift z, r_Δ is the radius of a sphere around the halo centre enclosing a mean density of Δ times the critical density $\rho_\mathrm{c}(z)$ of the Universe at redshift z. The mass inside r_Δ is

$$M_\Delta = \rho_\mathrm{c}\Delta\frac{4}{3}\pi r_\Delta^3. \quad (2)$$

According to the spherical collapse model in an Einstein-de Sitter universe, r_Δ is the halo's virial radius at all redshifts if $\Delta = 18\pi^2 \approx 178$ (Peebles 1980; Eke et al. 1996). In more general cosmologies, the virial overdensity Δ will depend on redshift and on the cosmological parameters. Useful fitting formulae exist (Lacey & Cole 1993; Eke et al. 1996; Bryan & Norman 1998), but we follow the common practice to define halo masses M_{200} and radii r_{200} here through an overdensity of $\Delta = 200$. Although they are not virial quantities, they are used because they are independent of redshift and cosmological parameters and adequately describe regions in virial equilibrium.

Accordingly, we define the concentration parameter by $c = r_{200}/r_\mathrm{s}$. In terms of c, the scale radius and the scale density can be expressed as

$$r_\mathrm{s} = \left(\frac{3M_{200}}{800\pi\rho_\mathrm{c}c^3}\right)^{1/3} \quad \text{and} \quad \rho_\mathrm{s} = \frac{200}{3}\rho_\mathrm{c}\frac{c^3}{F(c)} \quad (3)$$

respectively, where

$$F(c) = \ln(1 + c) - \frac{c}{1 + c}. \quad (4)$$

Halo mass and concentration can thus replace the scale radius and the scale density as the two parameters fully describing the halo density profile.

It has been firmly established in numerical simulations and observations (Wu & Xue 2000; Buote et al. 2007; Comerford & Natarajan 2007) that the halo concentration decreases with the halo mass. This is usually explained by the fact that low-mass halos form earlier than massive halos in the hierarchical structure-formation scenario in a CDM universe, and the assumption that the central halo density reflects the mean cosmic density at the formation redshift. This explains why massive haloes are typically found to be less concentrated than low-mass halos. The average relation between mass and concentration allows us to characterise halos by a single parameter, usually taken to be the virial mass M_{200}.

2.2. Concentration

Three different algorithms were proposed in the past to relate the concentration to the virial mass of a dark matter halo.

The first, by Navarro et al. (1997), defines the formation redshift z_c of a dark-matter halo of mass M_{200} collapsed at redshift z as the redshift when half of the final mass was first contained in progenitors more massive than some fraction f of M_{200}.

Based on the extended Press-Schechter formalism (Press & Schechter 1974; Bond et al. 1991; Lacey & Cole 1993), z_c can then be evaluated as a function of f, z and the final mass M_{200}. In line with hierarchical structure formation, NFW assumed the scale density, which depends only on c once the cosmology is fixed, to be directly proportional to the mean matter density of the universe at z_c, with a proportionality constant C. They showed that the c-M relation found in a set of numerically simulated, relaxed dark matter halos at $z = 0$ is well reproduced if $f \approx 0.01$ and $C \approx 3 \times 10^3$. This holds for several different cosmological models and initial density-fluctuation power spectra.

Bullock et al. (2001) confirmed that this algorithm works well for $z = 0$, but predicts too high halo concentrations at higher redshifts. They require that the typical halo mass $M_*(z_\mathrm{c})$ at the halo-formation redshift z_c be a fixed fraction f of the final halo mass M_{200}. They also relate the scale density of the halo to the critical density at the formation redshift, but use a different definition for the scale density. The concentration found in this way scales with redshift as $c \propto (1 + z)^{-1}$, in contrast to the much shallower redshift dependence in the NFW algorithm.

Finally, Eke et al. (2001) proposed an alternative explanation for the c-M relation, using a single parameter instead of the two parameters C and f and avoiding problems of the algorithm by Bullock et al. (2001) with the truncated power spectra of Warm Dark Matter cosmogonies.They define the halo-formation redshift z_c implicitly by

$$D_+(z_\mathrm{c})\sigma(M_\mathrm{s})\left[-\frac{\mathrm{dln}\,(\sigma)}{\mathrm{dln}\,M}(M_\mathrm{s})\right] = \frac{1}{C}, \quad (5)$$

where M_s is the mass contained within $2.17r_\mathrm{s}$, the radius of maximum circular velocity for the NFW density profile, $\sigma(M)$ is the standard deviation of density fluctuations on the mass scale M, and $D_+(z)$ is the linear growth factor. They then equate the scale density as defined by Bullock et al. (2001) to the spherical collapse top-hat density at the formation redshift.

The c-M relation by Eke et al. (2001) is probably the most general and physically best motivated. It makes use of a single fit parameter and turned out to reproduce halo concentrations in a variety of cosmologies, including those with dynamical dark energy (Dolag et al. 2004). It reproduces the results of the algorithm by Bullock et al. (2001) for galaxy-sized objects, but reveals significant differences on cluster scales, as we shall see later on.

At fixed halo mass and formation redshift, the concentration parameters of numerically simulated dark-matter halos are log-normally distributed around the median value c_0 reproduced by the algorithms described above,

$$p(c)\mathrm{d}c = \frac{1}{\sigma_\mathrm{c}\sqrt{2\pi}}\exp\left[-\frac{(\ln c - \ln c_0)^2}{2\sigma_\mathrm{c}^2}\right]\mathrm{dln}\,c, \quad (6)$$

with a standard deviation of $\sigma_\mathrm{c} \approx 0.2$ (Jing 2000; Bullock et al. 2001; Dolag et al. 2004).

The log-normal distribution (6) is skewed towards high concentrations. Its maximum occurs at $c_\mathrm{m} = c_0\exp\left(-\sigma_\mathrm{c}^2\right) < c_0$, and

the probabilities for $c < c_0$ and $c \geq c_0$ are equal. The mean concentration is (Coles & Jones 1991)

$$\mu_1 = c_0 \exp\left(\sigma_c^2/2\right), \tag{7}$$

its variance is

$$\mu_2 = \mu_1 \left[\exp\left(\sigma_c^2\right) - 1\right], \tag{8}$$

and the skewness is

$$\mu_3 = \frac{1}{\mu_1^3} \frac{\exp\left(3\sigma_c^2\right) - 3\exp\left(\sigma_c^2\right) + 2}{\left[\exp\left(\sigma_c^2\right) - 1\right]^3}. \tag{9}$$

Setting $\sigma_c = 0.2$, we find $\mu_3 \simeq 70/c_0^3 > 0$, showing that the distribution (6) is substantially skewed towards high c. Thus the probability of finding concentrations $c \gg c_0$ is considerably larger than for $c \ll c_0$. This is also seen when computing the ratio of the absolute deviations $|c - c_0|$ for $c > c_0$ and $c < c_0$, which is

$$\frac{\langle|c - c_0|\rangle_+}{\langle|c - c_0|\rangle_-} = \frac{\mathrm{erf}\left(\sigma_c/\sqrt{2}\right) + \left[1 - \exp\left(-\sigma_c^2/2\right)\right]}{\mathrm{erf}\left(\sigma_c/\sqrt{2}\right) - \left[1 - \exp\left(-\sigma_c^2/2\right)\right]}, \tag{10}$$

with the error function $\mathrm{erf}(x)$. For $\sigma_c = 0.2$, this ratio becomes $\approx$1.28, indicating that the absolute deviation for $c > c_0$ is on average $\approx$30% larger than for $c < c_0$. We shall return later to this issue to explain some of our lensing statistics results.

3. Cluster population

We model the galaxy-cluster population using one of the merger-tree sets produced for the earlier study by Fedeli & Bartelmann (2007a). Extended Press-Schechter theory was used to reproduce the formation history of $\mathcal{N} = 500$ dark-matter halos in four different dark-energy cosmologies. Here, we only use the merger tree constructed for the concordance ΛCDM model, whose parameters were set to $\Omega_{\mathrm{m},0} = 0.3$, $\Omega_{\Lambda,0} = 0.7$, $h = 0.65$ and $\sigma_8 = 0.84$. At redshift zero, the halos are drawn *uniformly* from the mass interval between 10^{14} and $2.5 \times 10^{15}\ M_\odot\, h^{-1}$ to achieve a good coverage of the mass range relevant for strong lensing. For details on the Monte-Carlo generation of merger trees and their applications, we refer the reader to Somerville & Kolatt (1999); Randall et al. (2002); Cassano & Brunetti (2005); Fedeli & Bartelmann (2007a,b).

Each dark-matter halo in the sample is evolved in a number of discrete redshift steps starting from the present time up to a source redshift z_s randomly drawn from the observed distribution of faint blue galaxies parameterised by Smail et al. (1995; see also Bartelmann & Schneider 2001). This distribution peaks at $z_s \simeq 1.2$, rendering the region around $z_l \simeq 0.3$–0.5 the most geometrically efficient for gravitational lensing.

At each discrete redshift step between redshifts zero and z_s, the merger tree of an individual halo contains the halo mass itself and a randomly assigned mass increment compared to the previous redshift step. This quantifies the magnitude of the merger or smooth accretion process the halo is undergoing within the respective time interval.

As in Fedeli & Bartelmann (2007a), we twice compute the strong-lensing efficiency of each dark-matter halo at each redshift step, first assuming that the halo can be characterised by an unperturbed NFW density profile with elliptical isopotential contours (we choose $e = 0.3$ for the ellipticity, in agreement with Meneghetti et al. 2003b), and a second time including the merger process experienced by the halo.

Given the mass and the redshift of a halo in the sample, we use the algorithm by Eke et al. (2001) to compute the nominal concentration $c_0(M, z)$. Again, we distinguish two cases in the strong-lensing analysis, assigning either the nominal concentration c_0 to the halo or a value drawn randomly from the log-normal distribution (6) with a standard deviation $\sigma_c = 0.2$ about c_0.

We thus carry out four strong-lensing analyses for all halos in our $\mathcal{N} = 500$ merger trees, ignoring or including the effects of merger events and the scatter of the concentration about its nominal value set by the c-M relation.

Note that this Monte-Carlo generation of merger trees should be considered as a random experiment, representative of the evolution history of the entire cluster population. In line with this view, we draw a new value of the concentration at each new redshift step for each dark-matter halo.

The lensing efficiency for a single halo is quantified by the cross section σ_d, that is the area of the domain on the source sphere in which a source has to lie in order to produce at least one gravitational arc with a length-to-width ratio $\geq d$. We calculate the cross sections using the semi-analytic algorithm described in Fedeli et al. (2006). It allows to rapidly compute strong-lensing efficiencies for realistic source distributions, and yields results that are in good agreement with those of costly, fully-numerical ray-tracing simulations. We refer the reader to the quoted paper for details.

Having computed all cross sections for each of the four alternative assumptions on the internal structure and mergers experienced by the halos, we quantify the global lensing efficiency of the cluster population using the optical depth per unit redshift,

$$t_d(z) = \frac{\mathrm{d}\bar{\tau}_d(z)}{\mathrm{d}z} = \sum_{i=1}^{\mathcal{N}-1} \frac{\sigma_d(M_i, z, z_{s,i})}{4\pi D_{s,i}^2} \int_{M_i}^{M_{i+1}} \frac{\mathrm{d}^2 N(M, z)}{\mathrm{d}M\mathrm{d}z} \mathrm{d}M, \tag{11}$$

where $D_{s,i}$ is the angular diameter distance to the source sphere from the ith dark matter halo in the sample, while $\mathrm{d}^2N(M,z)/\mathrm{d}M\mathrm{d}z$ is the number of cosmic objects contained in the unit mass around M and in the unit redshift around z. The integral in (11) over the lens redshift gives the total average optical depth, which is proportional to the total number of arcs with length-to-width ratio larger than d predicted to be produced on the full sky.

The optical depth per unit redshift is simply a sum of the cross sections of each individual halo, weighted by the abundance of such halos at the corresponding redshift. Weighting by the mass function causes this sum to be dominated by the halos with the lowest masses that are still capable of producing a non-vanishing arc cross section. Introducing the scatter into the mass-concentration relation can lift low-mass halos above or push them below the strong-lensing threshold. However, the skewness of the concentration distribution makes it more likely that low-mass halos are lifted above the threshold than the reverse. Thus, it is plausible that the log-normal concentration distribution may have a potentially significant effect on the strong-lensing optical depth.

4. Results

4.1. Different concentration prescriptions

Before we continue, it is interesting to assess how the strong-lensing cross sections differ for the different c-M relation algorithms outlined in Sect. 2. At the same mass and redshift, higher

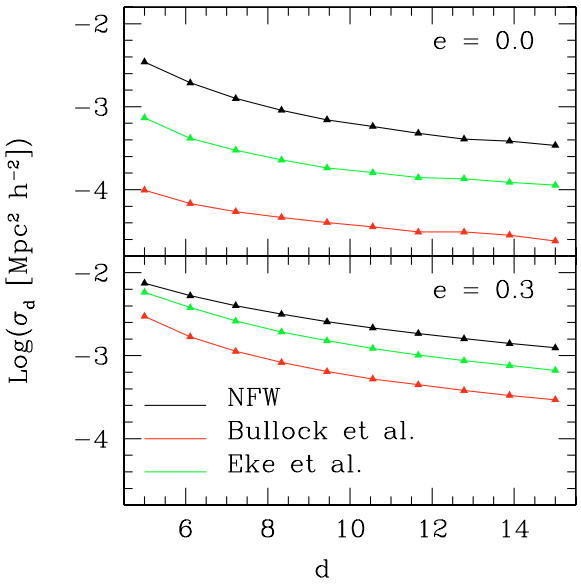

Fig. 1. The cross section for arcs with length-to-width ratio $\geq d$ is shown as a function of d. The mass of the lensing halo is $2 \times 10^{15}\ M_{\odot}\, h^{-1}$, the lens redshift is $z_l = 0.3$ and the source redshift is $z_s = 1$. Results for three different prescriptions for c-M relation are presented as labeled in the plot. The two panels show results for axially-symmetric (*top*) and elliptical (*bottom*) lenses with an isopotential ellipticity of $e = 0.3$.

concentrations should push the critical curves of a lensing halo outwards, thus increasing its strong-lensing cross section.

Results are shown in Fig. 1, where we plot the cross section for gravitational arcs with length-to-width ratios $\geq d$ as a function of d, using the three algorithms for the c-M relation. We also show the difference between axially-symmetric and elliptical lenses.

Evidently, the impact of different concentrations is much reduced for elliptical compared to circular lenses. For example, if we focus on $d = 10$, we note that the cross sections differ by a factor of $\approx$4 for elliptical lenses. For axially-symmetric lenses, this factor grows up to $\approx$20. This is owed to the fact that halo ellipticity largely increases the strong-lensing cross section (Meneghetti et al. 2003b; Oguri et al. 2003; Meneghetti et al. 2007), causing the lensing efficiency to be less sensitive to the internal structure of the lens.

Next, we see that the original NFW prescription for the c-M relation yields the largest cross sections for all values of d. As explained in Sect. 2, this is because the NFW prescription performs well at redshift zero, but overpredicts concentrations at higher redshift. At $z = 0.3$, where we placed the lens, the concentration is thus substantially overestimated, resulting in a very large cross section.

Concentrations computed using Bullock et al. (2001) and Eke et al. (2001) algorithms agree on galactic scales, but differ on cluster scales. Although results obtained with them both fall below the NFW result, they produce quite different cross sections for all d. In particular, the Eke et al. (2001) algorithm yields results falling in between those obtained with the NFW and Bullock et al. (2001) prescriptions, respectively.

This illustrates that the choice of the c-M relation is very important in analytic and semi-analytic models of galaxy-cluster lensing since different concentrations can have a large effect on the strong-lensing properties. The factors exceeding one order of magnitude between different prescriptions shown in Fig. 1 for axially symmetric lenses is particularly striking in this regard.

We compared strong-lensing cross sections for several dark-matter halos extracted from a high-resolution numerical simulation with those of analytic lens models with NFW density profile with the same mass and redshift, an isopotential ellipticity of 0.3 and with each of the three different algorithms for the c-M relation. We generally find the best agreement of the strong-lensing efficiencies for concentrations computed with the algorithm by Eke et al. (2001). This further supports the plausibility of this algorithm for the c-M relation. From now on, we assign fiducial concentrations by means of the Eke et al. (2001) algorithm for the c-M-relation.

4.2. Scatter in the concentration

We now proceed as anticipated in Sect. 3, performing four different strong-lensing analyses for our dark-matter halo population.

We show in Fig. 2 the optical depth per unit redshift as a function of lens redshift as defined in Eq. (11), for arcs with length-to-width ratios $d \geq 7.5$ and $d \geq 10$ respectively. Results are shown both including and ignoring the effect of cluster mergers, and both assuming the ideal c-M relation and introducing a concentration scatter consistent with the log-normal distribution of Eq. (6).

For the two cases $d \geq 7.5$ and $d \geq 10$, we used two different seeds for drawing random concentrations from the distribution in order to gain insight into the effect of limited statistics.

We first note the general trend that the introduction of the scatter in the c-M relation systematically increases the optical depth, and this is true irrespective of whether halo mergers are taken into account or ignored. This is a consequence of the skewness of the concentration distribution; cf. Sect. 2. Since concentrations much larger than the fiducial value are more probable than much lower concentrations, it is more likely for the concentration scatter to increase the strong-lensing cross section rather than the reverse. In other words, halo concentrations become larger on average after introducing the scatter, thus producing a larger optical depth per unit redshift.

In closer detail, we note several local maxima of the differential optical depths per unit redshift obtained after introducing a scatter in the c-M relation. These are caused by individual dark-matter halos with relatively low mass that, due to the random assignment of concentrations, reach a particularly high concentration and thus a large cross section. Because of their low mass, they have a large relative abundance, thus they dominate the sum in the optical depth per unit redshift, Eq. (11), and cause the peaks.

The position, width and amplitude of these peaks change of course if the seed for the random-number generation is changed. However, even though the *local* increase in the differential optical depth can be quite significant, the increase in the *total* optical depth, i.e. the integral under the curves in Fig. 2, is limited to $\approx$40–50%, both including or ignoring halo mergers.

To study this in more detail, we concentrate on $d \geq 10$ and the more realistic case when mergers are taken into account. We further select a halo subsample with redshifts between $z_1 = 0.28$ and $z_2 = 0.32$, centred on $z = 0.3$. Since our original cluster sample was randomly drawn from a uniform mass distribution at $z = 0$ and then evolved backwards in time to construct merger trees, each dark-matter halo of mass M_{200} at redshift z needs to be statistically weighted by the abundance of such halos according to the mass function for the cosmological model at hand. We

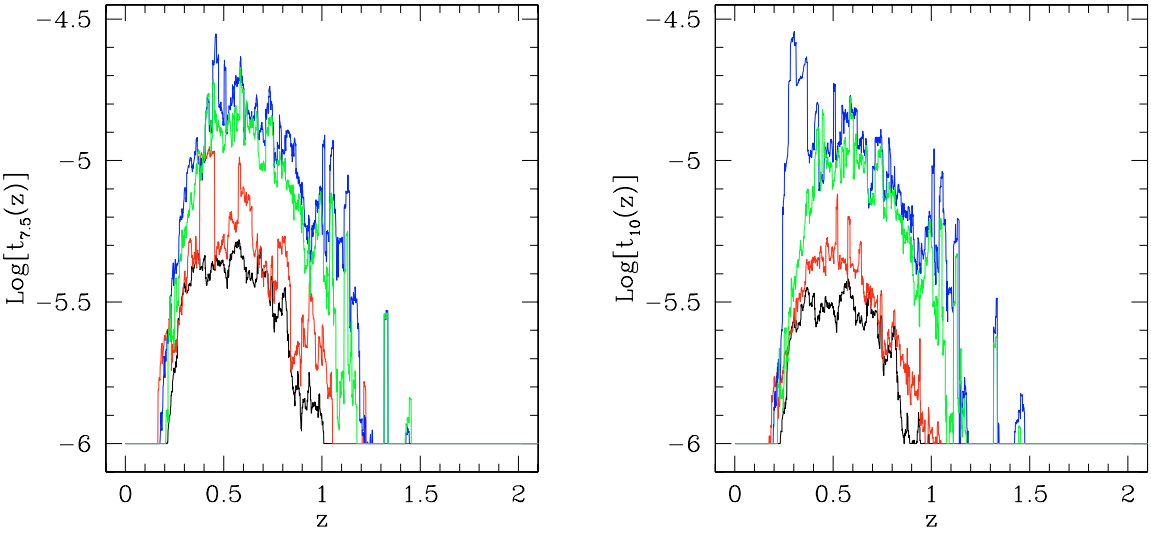

Fig. 2. *Left panel*. Optical depth per unit redshift for arcs with length-to-width ratio $d \geq 7.5$ as a function of the lens redshift. The thin black and green lines show the results obtained ignoring and accounting for cluster mergers, respectively, both using the nominal *c-M* relation. The heavy red and blue curves include the scatter in the *c-M* relation. *Right panel.* Similar to the left panel, but for arc length-to-width ratios $d \geq 10$, and using a different random-number seed.

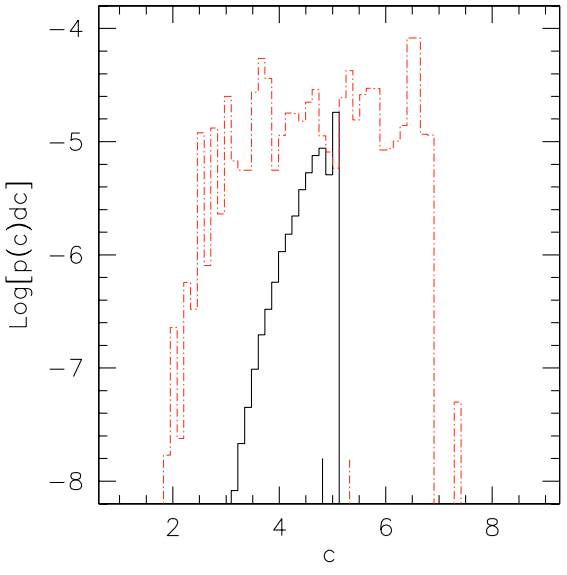

Fig. 3. Unnormalised distribution of the concentrations for all the halos in our sample with redshifts between $z_1 = 0.28$ and $z_2 = 0.32$. The black solid histogram shows the result obtained adopting the fiducial *c-M* relation of Eke et al. (2001). The log-normal concentration scatter is taken into account for the red-dashed histogram. The vertical dashes indicate the median concentration in both cases.

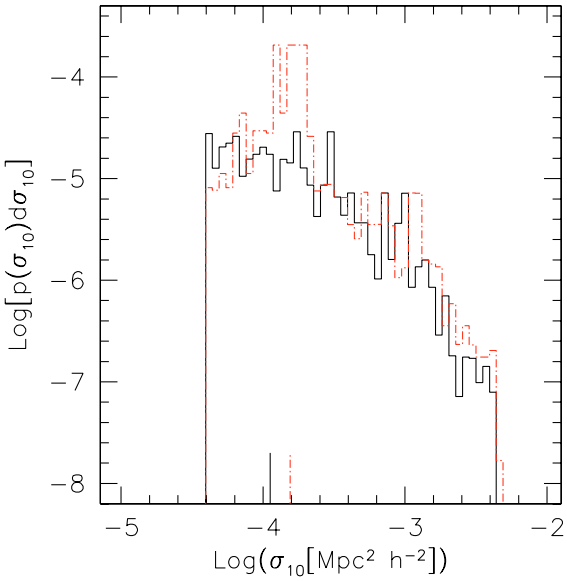

Fig. 4. Unnormalised distribution of the cross sections for gravitational arcs with length- to-width ratios $d \geq 10$ for all halos in our subsample with redshifts between $z_1 = 0.28$ and $z_2 = 0.32$. As in Fig. 3, the black solid and red dashed histograms show results ignoring the concentration scatter and accounting for it, respectively. Dashed vertical lines mark the median cross sections for both cases.

note that appropriate weights are included in the optical-depth calculations, see Eq. (11).

Figures 3 and 4 show the distributions of concentrations and strong-lensing cross sections in the halo subsample. In both figures, we contrast results obtained ignoring the concentration scatter (solid black curves) and taking it into account (red dashed curves). Note that all distributions shown are unnormalised.

Without scatter, the concentration distribution is very peaked, but it flattens and widens when the scatter is taken into account, as one would expect. Note also that both concentration distributions drop very sharply at high concentrations. This reflects the mass cutoff in our halo sample, since high concentrations correspond to low masses.

The cross-section distributions behave similarly. However, in this case the sudden cut-off at low cross sections is due to the strong-lensing threshold. For producing large arcs, a halo's caustics need to be sufficiently larger than the available sources. Below this threshold, the strong-lensing cross sections sharply drop to zero. See also Fedeli et al. (2006) for more discussion of this issue and its implementation.

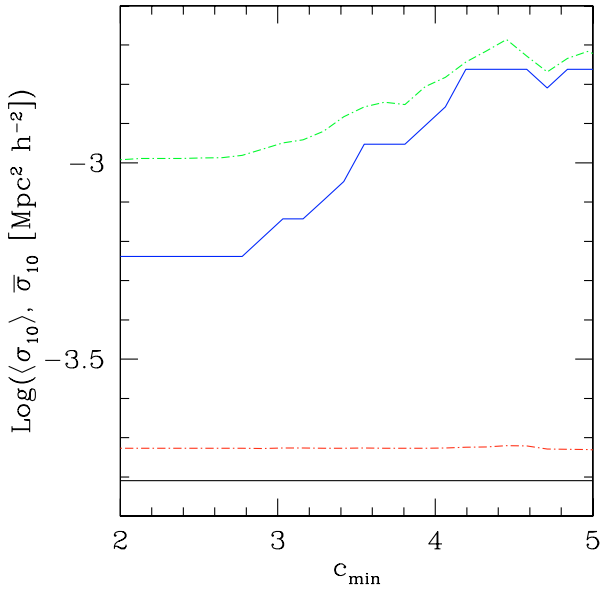

Fig. 5. The black and blue solid curves show the median, and the red and green dashed curves the mean cross section for arcs with length-to-width ratio $d \geq 10$. Only halos with concentrations above the threshold on the abscissa are included. The bottom pair of lines shows the result without any mass selection, while only halos more massive than $7.5 \times 10^{14}\ M_\odot\, h^{-1}$ are included in the top pair.

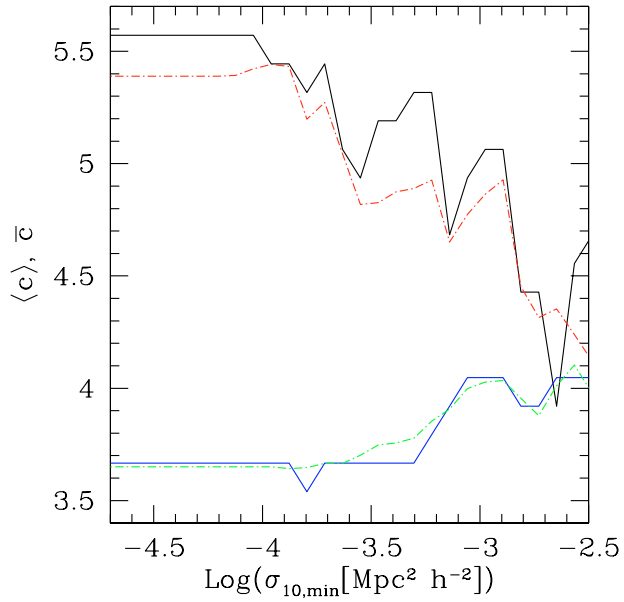

Fig. 6. The black and blue solid curves show the median, the red and green dashed curves the mean concentration. Only halos with strong-lensing cross sections above the threshold on the abscissa are taken into account. The top pair of curves shows the result obtained without mass selection, while only halos more massive than $7.5 \times 10^{14}\ M_\odot\, h^{-1}$ contribute to the bottom pair of curves.

Finally, the systematic increase of the differential optical depth shown if Fig. 2 can be further understood as the contribution of two factors. First, we note that the median concentration (and hence also the median strong-lensing cross section) is larger when the concentrations scatter about the mean c-M relation. Second, the significant peaks in Fig. 4 (note the logarithmic scale!) appearing in the cross-section distribution at relatively low cross sections are produced by rather low-mass halos that dominate the sum in the optical depth per unit redshift because of their large statistical weight.

4.3. Lensing concentration bias

Another interesting issue that we are able to explore with our halo sample regards the strong-lensing cross sections expected for concentrated halos, and conversely the concentrations expected in efficient strong-lensing halos.

This will allow us to better understand the relative effect of mass and concentration on the amplitude of the strong lensing cross section, and to quantify the bias expected to be found in dark-halo concentration measurements of strongly-lensing clusters. We can then compare such results to those obtained by Hennawi et al. (2007), who carried out among other things a similar analysis on a large set of numerically simulated dark-matter halos.

Figure 5 shows the median $\overline{\sigma}_{10}$ and the mean $\langle\sigma_{10}\rangle$ cross sections of the halo subsample, restricted to those halos with a concentration exceeding the threshold on the abscissa. Results are shown both for all halos irrespective of their mass, and only for halos with masses $\geq 7.5 \times 10^{14}\ M_\odot\, h^{-1}$.

Without mass selection, the curves are flat within the range of concentrations shown. Remarkably, this indicates that low-mass halos with their typically high concentrations have similar mean or median cross sections as high-mass halos and therefore contribute most of the strong-lensing optical depth in the halo subsample because of their high abundance.

This result may seem at odds with the expectation that the lensing efficiency should increase with increasing halo concentration, as illustrated in Fig. 1 when we discussed the effect of different algorithms implementing the c-M relation. However, note that Fig. 1 shows results for a single halo mass. If we select only the most massive halos, we find an increase of the mean and median cross sections with the concentration threshold. Thus, once the mass dependence is effectively suppressed in this way, the concentration dependence of the strong-lensing efficiency can emerge. In other words, although the average strong-lensing cross sections do indeed increase with the halo concentration, this effect is almost precisely cancelled if halos of all masses in a broad mass range are considered.

According to Fig. 5, the median and mean cross sections of massive halos can increase by a factor of ≈2.5 as the concentration increases from 2 to 5.

Figure 6 shows the mean $\langle c\rangle$ and median $\bar{c}$ concentration of halos with strong-lensing cross sections above the threshold on the abscissa. Again, we compare the complete halo subsample with massive halos above a mass limit of $7.5 \times 10^{14}\ M_\odot\, h^{-1}$. We note that (i) if we impose no mass threshold, the concentration for strongly lensing halos is always smaller on average compared to the entire population, and (ii) if we allow only massive halos, the mean and median concentrations increase with the lensing cross section.

Specifically, the mean and median concentrations of massive halos shown in Fig. 6 increase by ≈12% across the range of cross-section thresholds shown. If we further raise the mass threshold, the increase rises to ≈25%.

Without any mass selection, the highest cross sections are produced by the most massive objects, that are on average less concentrated than the low-mass halos. If we restrict the analysis

to massive halos, we remove part of the mass dependence of the strong-lensing efficiency and find that the concentrations found in strongly lensing clusters are slightly biased high. Narrowing the mass interval, the effect of the concentration is less diluted by the mass dependence, thus increasing the bias. This result agrees with the corresponding result of Hennawi et al. (2007) and will be discussed later on.

4.4. X-ray concentration bias

It is now interesting to ask whether comparable concentration biases are expected in X-ray selected cluster samples. At fixed mass, a more concentrated halo creates a deeper potential well and thus causes the intracluster gas to become hotter in thermal and hydrostatic equilibrium. The gas density will also increase, thus raising the X-ray luminosity.

To address this question, we first require a relation between the X-ray observables and mass, the redshift and the concentration of the host dark-matter halo. We achieve this following Eke et al. (1998) who derived an extension to the usual cluster scaling relations (White & Rees 1978; White 1982; Kaiser 1986). First of all, the circular velocity profile for a dark-matter halo with an NFW density profile is (Navarro et al. 1997)

$$\left[\frac{v(r)}{v_{200}}\right]^2 = \frac{r_{200}}{r}\frac{F(cr/r_{200})}{F(c)}, \tag{12}$$

where v_{200} is the circular velocity at r_{200}, that is $v_{200}^2 = GM_{200}/r_{200}$. This distribution peaks at $r \approx 2r_{200}/c$, corresponding to

$$v_{\rm m}^2 \approx 0.22 v_{200}^2 \frac{c}{F(c)}. \tag{13}$$

This characteristic velocity of the system measures the depth of its potential well. If only gravity or other scale-free processes like pressure gradients or hydrodynamical shocks dominate within the cluster, any other measure of the potential depth, such as the temperature of the intra-cluster gas, must be proportional to $v_{\rm m}^2$, that is

$$T(M_{200}, z, c) \propto \frac{M_{200}}{r_{200}}\frac{c}{F(c)}. \tag{14}$$

Now, Eq. (2) implies

$$r_{200} = \left[\frac{3M_{200}}{800\pi\rho_c(z)}\right]^{1/3}. \tag{15}$$

Inserting this into Eq. (14), we can write

$$T(M_{200}, z, c) = \beta\,[M_{200}h(z)]^{2/3}\frac{c}{F(c)}, \tag{16}$$

where β collects now all the constant factors. Note that this relation retains the mass and redshift dependence of the temperature of the common scaling relation, but acquires the concentration dependence from the dark-matter density profile. In particular, the function $c/F(c)$ is a monotonically increasing function of the concentration if $c \gtrsim 2$, which is almost always the case in our halo sample (cf. the concentration distribution in Fig. 3). It is shown that adiabatic simulations of gas in galaxy clusters follow relatively well this type of scaling relation (Eke et al. 1998; Bryan & Norman 1998). With the introduction of more complex physical processes, like non gravitational heating and radiative cooling, the scaling relation is instead not closely reproduced (Babul et al. 2002; Kay et al. 2002). However, in spite of simplicity, we prefer to stick to it, leaving more complicated models for further study.

Quantifying the bolometric X-ray luminosity of the intracluster gas, we start from

$$L_{\rm X}(M_{200}, z, c) = 4\pi\int_0^{+\infty} r^2\rho_{\rm g}(r)^2\frac{\Lambda(T)}{(\mu m_{\rm p})^2}{\rm d}r, \tag{17}$$

where $\Lambda(T)$ is the cooling function, depending on the relevant radiative processes, and $\rho_{\rm g}(r)$ is the gas-density profile. We assume that the gas density follows the dark matter density, $\rho_{\rm g} = f_{\rm g}\rho$, with a constant factor constant $f_{\rm g}$. This is of course not strictly true, especially in the inner region where the dark-matter density profile is cuspy while the gas distribution forms a finite core due to the gas pressure. However, the final result is insensitive to this simplifying assumption. Further assuming that the intracluster gas is isothermal, the luminosity can be written as

$$L_{\rm X}(M_{200}, z, c) = 200\Lambda(T)\left(\frac{f_{\rm g}}{3\mu m_{\rm p}}\right)^2 M_{200}\rho_{\rm c}(z)\frac{c^3}{F(c)^2}. \tag{18}$$

If the main emission mechanism of the intra-cluster gas is thermal bremsstrahlung, then $\Lambda(T) \propto T^{1/2}$. Hence, recalling Eq. (16) and collecting all constant factors into γ, we get

$$L_{\rm X}(M_{200}, z, c) = \gamma M_{200}^{4/3}h(z)^{7/3}\frac{c^{7/2}}{F(c)^{5/2}}. \tag{19}$$

The common dependence of the luminosity on the mass and the redshift of the host dark matter halo is retained again, and an additional dependence on the concentration appears. Note that the concentration dependence is steeper here than for the temperature. Note that the dependence of the bolometric X-ray luminosity on the concentration shown in Eq. (19) differs by a factor of $1-(1+c)^{-3}$ from the formula given in Eke et al. (1998). This is because the integral in Eq. (17) extends to infinity, while it was limited to the virial radius in Eke et al. (1998). This is unimportant because the missing factor is very close to unity for all reasonable values of the concentration.

In the following, we refer the temperature and the X-ray luminosity of the gas inside each dark-matter halo of our subsample to the temperature $T_{\rm r}$ according to (16) and the luminosity $L_{X,{\rm r}}$ according to (19) of a reference halo with mass $M_{200,{\rm r}} = 10^{15}\ M_\odot\, h^{-1}$ placed at redshift $z_{\rm r} = 0$. It has a nominal concentration $c_{\rm r} = 3.74$ according to the Eke et al. (2001) algorithm. Thus, for each halo, we only consider the relative temperature

$$\frac{T(M_{200}, z, c)}{T_{\rm r}} = \left[\frac{M_{200}h(z)}{M_{200,{\rm r}}h}\right]^{2/3}\frac{c}{F(c)}\frac{F(c_{\rm r})}{c_{\rm r}}, \tag{20}$$

and the relative luminosity

$$\frac{L_{\rm X}(M_{200}, z, c)}{L_{\rm X,r}} = \left(\frac{M_{200}}{M_{200,{\rm r}}}\right)^{4/3}\left[\frac{h(z)}{h}\right]^{7/3}\frac{c^{7/2}}{F(c)^{5/2}}\frac{F(c_{\rm r})^{5/2}}{c_{\rm r}^{7/2}}. \tag{21}$$

Figure 7 shows the median and mean concentrations for dark-matter halos with a relative gas temperature exceeding the threshold on the abscissa. We show the results both without any mass selection and selecting halos more massive than $7.5\times 10^{14}\ M_\odot\, h^{-1}$. Evidently, the mean and median halo concentrations decrease in both cases as the relative temperature threshold increases. This illustrates that particularly hot gas resides in the most massive halos, quite irrespective of the concentration. Also, if we consider only the most massive objects, a plateau appears

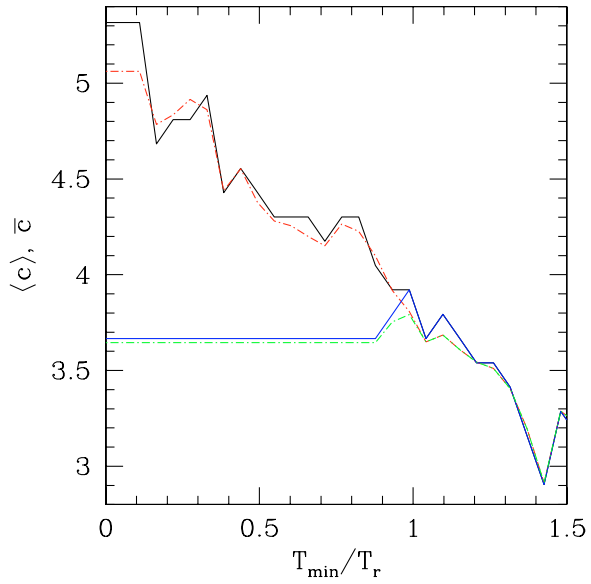

Fig. 7. Black and blue solid curves show the median, red and green dashed curves the mean concentration for the subsample of dark-matter halos between $z_1 = 0.28$ and $z_2 = 0.32$. Only halos with relative temperatures exceeding the threshold on the abscissa are included. The top pair of curves shows the result without mass selection, while only halos with mass larger than $7.5 \times 10^{14}\ M_\odot\, h^{-1}$ contribute to the bottom pair.

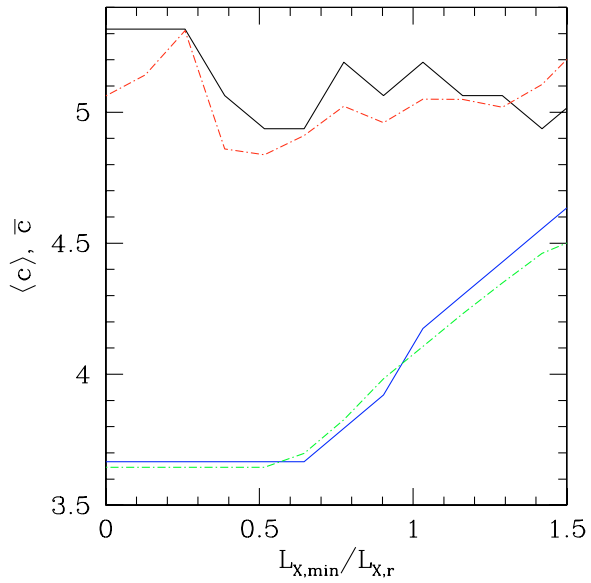

Fig. 8. Black and blue solid curves show the median, red and green dashed curves the mean concentration for the subsample of dark-matter halos between $z_1 = 0.28$ and $z_2 = 0.32$. Only halos with relative X-ray luminosities exceeding the threshold on the abscissa are taken into account. The top pair of curves was obtained without mass selection, while only massive halos with mass larger than $7.5 \times 10^{14}\ M_\odot\, h^{-1}$ contribute to the bottom pair.

at low temperatures because low-temperature clusters are then removed from the sample. Thus, the gas temperature depends so weakly on the halo concentration compared to its dependence on mass that even a narrow mass selection does not reveal the increasing concentration-temperature relation.

Figure 8 shows the mean and median concentrations in halos selected for their X-ray luminosity. If all halos in the subsample

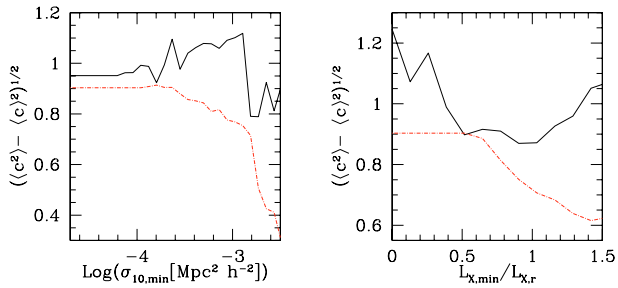

Fig. 9. The rms of the concentration distribution accounting for halos in the subsample with strong-lensing cross sections (*left panel*) or relative X-ray luminosities (*right panel*) exceeding the thresholds on the abscissa. The solid black lines are obtained without mass selection, while only massive halos with mass larger than $7.5 \times 10^{14}\ M_\odot\, h^{-1}$ contribute to the red dashed curves.

are included, the curves are almost flat, showing that the concentrations are typically independent of the X-ray luminosity. If only massive halos are included, the mean and median concentrations increase such that the most luminous X-ray clusters can be up to ≈25% more concentrated than the entire cluster population.

Hence, unlike for the temperature, we here find increasing mean and median concentrations as a function of the luminosity threshold. In summary, a concentration bias in temperature-selected clusters is not expected, but the most massive and X-ray luminous clusters are typically more concentrated than the population of X-ray clusters indicating a concentration bias similar to that found in strongly-lensing clusters.

The different results for clusters selected by temperature or X-ray luminosity can be understood considering the following numbers. As remarked before, the nominal concentration of the reference cluster is $c_r = 3.74$. Had we adopted a reference mass of $2.5 \times 10^{14}\ M_\odot\, h^{-1}$, the nominal concentration was $c_r = 4.73$. These two concentrations are 1-σ compatible with the same underlying mass, given the variance of $\sigma_c = 0.2$ in the log-normal concentration distribution. The increase in the gas temperature due to the higher concentration is only ≈5%, while the X-ray luminosity increases by ≈45%. On the other hand, the gas temperature drops by a factor of ≈2.5 because of the lower halo mass, while the bolometric X-ray luminosity drops by a factor of ≈6.3. On the whole, the ratio between the changes in temperature due to the halo mass and due to the concentration is ≈12, while the ratio between the changes in X-ray luminosity due to the mass and due to the concentration is ≈1.9. This shows that the effect of the concentration on the X-ray luminosity is almost comparable to the effect of the mass, but much less important for the temperature.

In other words, the mass dependence of the gas temperature is overwhelmingly stronger than its concentration dependence, cancelling any kind of concentration bias that could appear in temperature-selected halos. Very hot clusters are actually less concentrated (more massive) than average. On the other hand, the stronger dependence of the luminosity on the concentration allows to invert this trend if only massive clusters are considered. Thus, very X-ray luminous clusters have higher mean and median concentrations than clusters with lower luminosity but comparable mass.

To see which concentrations we can expect in suitably selected cluster samples, we plot in Fig. 9 the rms $(\langle c^2\rangle - \langle c\rangle^2)^{1/2}$ of the concentration distribution as a function of the cross-section and X-ray luminosity thresholds, respectively, both with and

without further mass selection. According to Figs. 6 and 8, the median and the mean of the distribution are quite similar, hence the distribution itself is quite symmetric, and the rms is a good estimator of its width.

Without mass selection, the rms always remains around unity. If we introduce mass selection, it is close to unity for the entire subsample, but drops towards 0.4 when only efficient strong lenses are included, and to 0.6 when only very X-ray luminous clusters are included. This means that the concentration distribution tends to narrow in the latter cases.

4.5. Additional effects

Finally, we explore the consequence for our results of two additional effects not included so far. The first is the correlation of the concentration with the triaxiality of dark-matter halos (Jing & Suto 2002). The second is the ellipticity distribution of projected halos due to the random orientation of the three-dimensional halos with respect to the line-of-sight (Oguri et al. 2003; Oguri et al. 2005; Corless & King 2006). The second effect affects only the strong lensing properties of galaxy clusters, for whose lensing potential we assumed an ellipticity of $e = 0.3$ throughout this work. The scaling laws we used for the X-ray characteristics are insensitive to the ellipticity of the dark-matter halo. Besides, the gas distribution approximately follows equipotential surfaces and thus tends to be more spherical than the dark matter distribution (Gavazzi 2005).

We assess the impact of these two effects in the following experiment. First, we considered a dark-matter halo with mass $2 \times 10^{15}\ M_\odot\, h^{-1}$ and redshift $z_l = 0.3$. We computed its cross section for arcs with length-to-width ratio $d \geq 10$, assuming sources at $z_s = 1$, a lensing-potential ellipticity $e = 0.3$ and concentration derived from the algorithm of Eke et al. (2001). Then, we produced 1000 triaxial modifications of this original halo by drawing axis ratios from the distributions given in Jing & Suto (2002). The axis ratios allow changing the concentration of each modified halo according to the prescription of Jing & Suto (2002), predicting higher concentrations for more spherical halos. Finally, each modified halo is projected along a randomly selected line-of-sight and the ellipticity of the projected density is computed following Oguri et al. (2003). To each halo is then assigned a new lensing-potential ellipticity assuming that it is half of the ellipticity of the projected density.

As outlined in Jing & Suto (2002), the isodensity surfaces tend to be more elongated near the core of the halo than in its outer regions. Since the innermost part of a galaxy cluster is most relevant for strong-lensing events, we lowered the minor-to-major and intermediate-to-major axis ratios by 0.15 prior to the projection. This is consistent with Fig. 3 of Jing & Suto (2002).

Cross sections were computed for each modified halo, using the new values of the concentration or of the ellipticty, or both. The three resulting cross-section distributions are shown in Fig. 10. The variation of the concentration with triaxiality introduces additional scatter in the cross section (red dot-dashed line), but significantly less than the concentration scatter introduced before. The small difference between the black solid and the green dashed curves in Fig. 10 corroborates this conclusion.

The distribution of cross sections obtained after random projections of triaxial halos is centered on the cross section for the original halo with fixed ellipticity $e = 0.3$, indicating that this lensing-potential ellipticity is typical. This confirms the result of Meneghetti et al. (2003b), who found this value by fitting the deflection angle maps of simulated galaxy clusters (see also

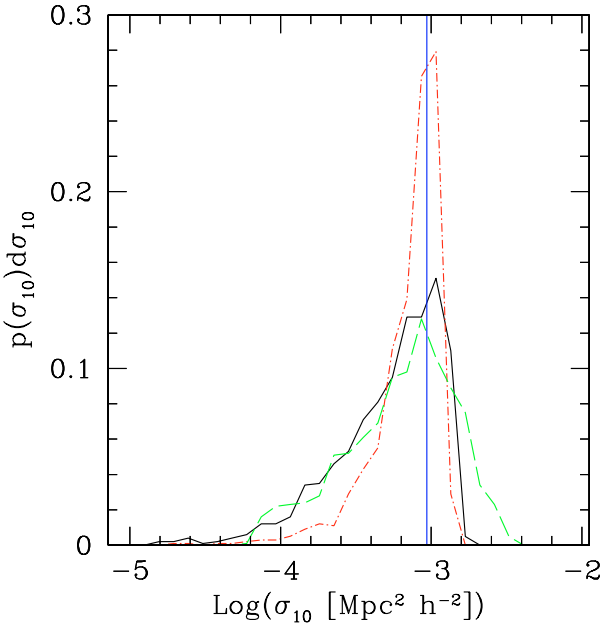

Fig. 10. Cross section distributions. The vertical blue line shows the cross section for arcs with length-to-width ratio $d \geq 10$ computed for a dark-matter halo of mass $2 \times 10^{15}\ M_\odot\, h^{-1}$ at redshift $z_l = 0.3$ with sources at redshift $z_s = 1$ and lensing-potential ellipticity $e = 0.3$. The red dot-dashed line is the distribution of the cross sections caused by the variation of halo concentrations with triaxiality. The green dashed line includes the ellipticity distribution of projected triaxial halos, and the black solid line contains both effects.

Meneghetti et al. 2005). The good agreement also shows that the reduced concentration of highly triaxial halos is compensated by the higher ellipticity.

The scatter caused by the ellipticity distribution exceeds that caused by the variation of the concentration with triaxiality, but the total scatter in the cross sections due to halo triaxiality shown in Fig. 10 is at most comparable to that caused by the intrinsic concentration distribution. Moreover, it does not systematically shift the cross sections towards higher or lower values, hence leaving unchanged the conclusions of this work. It should also be noted that these results are expected to hold if more detailed gas physics (such as cooling and star formation) is included because it tends to affect the inner slope rather than the ellipticity of the cluster mass distribution (Puchwein et al. 2005).

We have applied the same test to halos of different mass and found very similar results. The effect of the variation of halo concentrations with triaxiality on the temperature and luminosity of the X-ray gas is negligibly small.

5. Summary and discussion

We have investigated the effect of the scatter in the relation between concentration and mass in dark-matter halos on gravitational arc statistics and X-ray properties of galaxy clusters.

We have addressed the effect on strong-lensing cross sections of different implementations of the c-M relation proposed in the literature (Navarro et al. 1997; Bullock et al. 2001; Eke et al. 2001). We found substantial differences, with the algorithms by Navarro et al. (1997) and Bullock et al. (2001) predicting the highest and the lowest cross sections, respectively. We adopt the algorithm by Eke et al. (2001) because it needs only one instead of two free parameters, has been shown to be applicable to cosmological models with dynamical dark energy

(Dolag et al. 2004), and was found to yield strong-lensing results in good agreement with numerical simulations.

This result shows that caution must be applied when modelling galaxy cluster lenses with NFW density profiles, since different implementations of the *c*-*M* relation may yield largely different values for the lensing efficiency, in particular if axial symmetry is assumed.

We then used the Eke et al. (2001) algorithm to compute fiducial concentrations for a sample of $\mathcal{N} = 500$ dark-matter halos with masses between 10^{14} and $2.5\times10^{15}\,M_\odot\,h^{-1}$ at redshift zero. Each halo is evolved backwards in time in discrete redshift steps up to a source redshift randomly drawn for each halo from a parameterisation of the observed redshift distribution of faint blue galaxies. When the scatter in the concentration was taken into account, it was drawn from a log-normal distribution around the fiducial value, with a standard deviation of $\sigma_c = 0.2$. The effect of cluster mergers on the strong-lensing cross sections was also included (Torri et al. 2004; Fedeli et al. 2006), although the relative effect of the concentration scatter is insensitive to mergers.

The skewness of the log-normal distribution renders concentrations much above the fiducial value more likely than much below it, thus increasing on average the strong-lensing cross sections. Thus, the total optical depth, and hence also the total number of arcs expected on the sky, is increased by up to 50% by the concentration scatter. Moreover, the optical depth per unit redshift displays isolated significant peaks which are due to individual dark-matter halos with relatively low mass that happen to reach a particularly large concentration. Such halos can thus be turned into efficient lenses and contribute strongly to the optical depth because of their high abundance.

We then used our merger trees to better understand the relationship between dark-halo concentrations and their lensing efficiency. We found that selecting halos by concentration yields average cross sections similar to those of the complete sample. This shows that the higher concentrations of lower-mass halos compensates for their lower masses in terms of their strong-lensing efficiency until their caustic curves become too small compared to the sources to produce large arcs. Massive halos, however, reveal the concentration-dependence of the strong-lensing cross sections.

Conversely, the median and mean halo concentrations do not increase if the most efficient lensing halos are selected. However, selecting massive strong lenses reveals the dependence of the cross sections on the concentration, yielding median and mean concentrations increasing with the lensing efficiency. The most massive, strong lenses turn out to be 10–20% more concentrated than average lensing clusters.

This confirms a bias found earlier in numerically simulated clusters. Hennawi et al. (2007) found that strong cluster lenses have three dimensional concentrations ≈18% higher than typical clusters with similar mass. We found that the median concentration is ≈12% higher in halos with very high lensing efficiency compared to average halos with similar mass, and can grow up to 25% if massive clusters are selected.

Apart from the qualitative agreement, the quantitative agreement is quite reassuring especially in view of our different approach of modelling the halo population and its lensing efficiency semi-analytically compared to fully numerically. The 12% increase found here is certainly consistent with their 18% increase because a broader mass selection was applied here. Caution must thus be applied when extrapolating results on the inner structure of strongly lensing clusters to the entire cluster population.

Finally, we performed a similar analysis using the temperature and the bolometric luminosity of the X-ray emitting intracluster medium instead of the strong-lensing cross section. We assigned a temperature and an X-ray luminosity to each dark-matter halo in our sample by extending scaling relations first derived by Eke et al. (1998). They maintain the usual scalings $T \propto [M_{200}h(z)]^{2/3}$ and $L_X \propto M_{200}^{4/3}h(z)^{7/3}$, but include a dependence on the concentration of the host dark matter halo.

According to this analysis, there is no concentration bias in temperature-selected clusters, while a bias similar to strong lensing occurs for objects selected by their X-ray luminosity, if clusters of similar mass are selected. In particular, the mean and median concentrations of dark halos with increasing gas temperature decrease, reflecting that the temperature is much more sensitive to the halo mass than to its concentration. This result remains true when the halos are selected by mass. Likewise, dark halos with increasing X-ray luminosity have virtually unchanged concentrations if no mass selection is applied. If only massive objects are selected, the dependence of the bolometric luminosity on the concentration appears.

It is then an interesting question whether the two concentration biases due to strong lensing and X-ray luminosity conspire to produce a stronger effect. We computed the mean and median concentrations of clusters selected for strong lensing among those already selected for their X-ray luminosity and with mass larger than $7.5 \times 10^{14}\,M_\odot\,h^{-1}$. The further increase in concentration is very small compared to very X-ray luminous objects only. This is because selecting massive clusters for their high bolometric X-ray luminosity, we already select objects with high concentration that are typically also the most efficient lenses.

We also checked the effect of halo triaxiality on our results, which adds scatter to the halo concentrations and projected halo ellipticities, and, even though the latter is relatively significant, it leaves the conclusions of our paper unchanged.

These results confirm the general expectation that the gas temperature is more sensitive to the depth of the overall potential well and thus to the halo mass than to the internal halo structure. This does not hold true for the luminosity, which scales with the squared gas density and is thus substantially more sensitive to structural properties of the halo other than the mass. Similarly, the lensing efficiency is very sensitive to the details of the internal structure of the lens, as demonstrated in a variety of studies (Bartelmann et al. 1995; Meneghetti et al. 2003a,b; Oguri et al. 2003; Meneghetti et al. 2007).

Acknowledgements. This work was supported by the Collaborative Research Centre SFB 439 of the *Deutsche Forschungsgemeinschaft* and by the German Academic Exchange Service (DAAD) and the Conference of the Rectors of Italian Universities (CRUI) under the *Vigoni* programme. Part of the work has been performed under the Project HPC-EUROPA (RII3-CT-2003-506079) with support by the European Community – Research Infrastructure Action under the FP6 "Structuring the European Research Area" Programme. We thank the anonymous referee for useful comments that helped improving this paper.

References

Babul, A., Balogh, M. L., Lewis, G. F., & Poole, G. B. 2002, MNRAS, 330, 329
Bartelmann, M., & Schneider, P. 2001, Phys. Rep., 340, 291
Bartelmann, M., Steinmetz, M., & Weiss, A. 1995, A&A, 297, 1
Bond, J., Cole, S., Efstathiou, G., & Kaiser, N. 1991, ApJ, 379, 440
Bryan, G. L., & Norman, M. L. 1998, ApJ, 495, 80
Bullock, J., Kolatt, T., Sigad, Y., et al. 2001, MNRAS, 321, 559
Buote, D. A., Gastaldello, F., Humphrey, P. J., et al. 2007, ApJ, 664, 123
Cassano, R., & Brunetti, G. 2005, MNRAS, 357, 1313C
Coles, P., & Jones, B. 1991, MNRAS, 248, 1
Comerford, J. M., & Natarajan, P. 2007, MNRAS, 379, 190
Corless, V., & King, L. 2006 [arXiv:astro-ph/0611913]

Dolag, K., Bartelmann, M., Perrotta, F., et al. 2004, A&A, 416, 853
Dubinski, J., & Carlberg, R. G. 1991, ApJ, 378, 496
Eke, V., Cole, S., & Frenk, C. 1996, MNRAS, 282, 263
Eke, V. R., Navarro, J. F., & Frenk, C. S. 1998, ApJ, 503, 569
Eke, V., Navarro, J., & Steinmetz, M. 2001, ApJ, 554, 114
Fedeli, C., & Bartelmann, M. 2007a, A&A, 461, 49
Fedeli, C., & Bartelmann, M. 2007b [arXiv:astro-ph/0703789]
Fedeli, C., Meneghetti, M., Bartelmann, M., Dolag, K., & Moscardini, L. 2006, A&A, 447, 419
Gavazzi, R. 2005, A&A, 443, 793
Hennawi, J. F., Dalal, N., Bode, P., & Ostriker, J. P. 2007, ApJ, 654, 714
Jing, Y. 2000, ApJ, 535, 30
Jing, Y., & Suto, Y. 2002, ApJ, 574, 538
Kaiser, N. 1986, MNRAS, 222, 323
Kay, S. T., Pearce, F. R., Frenk, C. S., & Jenkins, A. 2002, MNRAS, 330, 113
Keeton, C. R., & Madau, P. 2001, ApJ, 549, L25
Kuhlen, M., Keeton, C. R., & Madau, P. 2004, ApJ, 601, 104
Lacey, C., & Cole, S. 1993, MNRAS, 262, 627
Meneghetti, M., Bartelmann, M., & Moscardini, L. 2003a, MNRAS, 346, 67
Meneghetti, M., Bartelmann, M., & Moscardini, L. 2003b, MNRAS, 340, 105
Meneghetti, M., Bartelmann, M., Jenkins, A., & Frenk, C. 2005 [arXiv:astro-ph/0509323]
Meneghetti, M., Argazzi, R., Pace, F., et al. 2007, A&A, 461, 25
Moore, B., Governato, F., Quinn, T., Stadel, J., & Lake, G. 1998, ApJ, 499, L5
Navarro, J., Frenk, C., & White, S. 1995, MNRAS, 275, 720
Navarro, J., Frenk, C., & White, S. 1996, ApJ, 462, 563
Navarro, J., Frenk, C., & White, S. 1997, ApJ, 490, 493
Navarro, J. F., Hayashi, E., Power, C., et al. 2004, MNRAS, 349, 1039
Oguri, M., Taruya, A., & Suto, Y. 2001, ApJ, 559, 572
Oguri, M., Lee, J., & Suto, Y. 2003, ApJ, 599, 7
Oguri, M., Takada, M., Umetsu, K., & Broadhurst, T. 2005, ApJ, 632, 841
Peebles, P. J. E. 1980, The large-scale structure of the universe (Princeton University Press)
Power, C., Navarro, J., Jenkins, A., et al. 2003, MNRAS, 338, 14
Press, W., & Schechter, P. 1974, ApJ, 187, 425
Puchwein, E., Bartelmann, M., Dolag, K., & Meneghetti, M. 2005, A&A, 442, 405
Randall, S. W., Sarazin, C. L., & Ricker, P. M. 2002, ApJ, 577, 579
Smail, I., Hogg, D. W., Yan, L., & Cohen, J. G. 1995, ApJ, 449, L105
Somerville, R. S., & Kolatt, T. S. 1999, MNRAS, 305, 1
Torri, E., Meneghetti, M., Bartelmann, M., et al. 2004, MNRAS, 349, 476
White, S. D. M. 1982, in Saas-Fee Advanced Course 12: Morphology and Dynamics of Galaxies, ed. L. Martinet, & M. Mayor, 12, 289
White, S. D. M., & Rees, M. J. 1978, MNRAS, 183, 341
Wu, X.-P., & Xue, Y.-J. 2000, ApJ, 529, L5
Wyithe, J., Turner, E., & Spergel, D. 2001, ApJ, 555, 504